NWRI CONTRIBUTION 87-68

A GENERALIZED APPROACH TO WIND SET-UP

by

Ioannis K. Tsanis

Visiting Fellow
Research and Applications Branch
National Water Research Institute
Canada Centre for Inland Waters
867 Lakeshore Road, P.O. Box 5050
Burlington, Ontario, Canada L7R 4A6

August 1987

MANAGEMENT PERSPECTIVE

The Management of large lakes requires information about the general circulation and short term water level variations. This paper describes a new analytical model for determining the wind setup and the drag coefficient for a lake. It provides an alternative approach to existing techniques.

Dr. J. Lawrence
Director, Research and Applications Branch
National Water Research Institute

PERSPERCTIVE - GESTION

La gestion de grands lacs nécessite des informations sur la circulation générale et sur les variations à court terme du niveau de l'eau. Le présent document décrit un nouveau modèle analytique visant à établir la montée du niveau de l'eau due aux vents et le coefficient de résistance pour un lac. Il apporte donc une solution de rechange face aux techniques existantes.

J. Lawrence
Directeur, Direction générale de la recherche et des applications
Institut national de recherche sur les eaux

RÉSUMÉ

La montée du niveau des nappes d'eau due aux vents est présentée d'une nouvelle façon faisant appel à des résultats analytiques et expérimentaux. Des solutions théoriques de la montée non dimensionnelle des eaux due aux vents dans des conditions d'interface air-eau lisses et très rugueuses montrant que la plupart des résultats obtenus en laboratoire et sur le terrain valent pour la zone de transition rugueuse. Une nouvelle approche analytique est présentée pour le coefficient de friction et les résultats sont vérifiés à l'aide d'expériences faites sur le terrain et en laboratoire.

A GENERALIZED APPROACH TO WIND SET-UP

Ioannis K. Tsanis
Visiting Fellow
National Water Research Institute
Canada Centre for Inland Waters
Burlington, Ontario, Canada

ABSTRACT

The wind set-up of water bodies is presented in a novel approach involving analytical and experimental results. Theoretical solutions for nondimensional wind set-up for smooth and fully rough air-water interface conditions delegate the majority of laboratory and field results in the transitionally rough region. A new analytical approach for the drag coefficient is presented and the results are verified by field and laboratory experiments.

INTRODUCTION

The wind acting on the water body surface generates waves and causes a surface current in the direction it blows, thus producing a windward lowering of the water level and a leeward rise, which is called wind set-up. Detailed knowledge of wind set-up in lakes and ocean bays is essential for flood control, safe navigation and shore protection.

Both field and laboratory experiments may be conducted to study the wind set-up. Model studies in the laboratory are very much simplified replicas of actual flows and are conveniently executed in systems combining air and water tunnels, i.e., "air-water" models. Simulation of this flow condition is possible with "solid-air" models where the shear stress is applied directly by a moving belt [6] or a moving bench seen from the moving bottomless box's reference system [13] while the sheared fluid is air, and the equivalent set-up is determined from the pressure gradient.

This paper provides new information by approaching the problem in a generalized way involving theoretical, laboratory and field results. In particular, analytical expressions for the wind set-up and the drag coefficient are presented and results from field experiments in the Great Lakes and from laboratory experiments are used for verification.

ANALYTICAL DEVELOPMENTS

For a steady two-dimensional condition depicted in Fig. 1a, the balance between shear stresses and pressure forces after disregarding terms higher than 0(dz), results in

$$\frac{dP}{dx} = \frac{dP_a}{dx} + \rho_w g \frac{d\zeta}{dx} = \frac{\tau_{sw} + \tau_{bw}}{h} \tag{1}$$

in which the subscript w stands for water, where $P = P_a + \rho_w g\,(h + \zeta)$ is the piezometric pressure, P_a is the atmospheric pressure, ρ_w is the water density, g is the acceleration due to gravity, h is the water depth, $\zeta = z - h$ is the displacement of the surface from the mean water level and τ_{sw} and τ_{bw} are the surface and bottom shear stresses, respectively, exerted on a fluid element of height z and length dx. Eq. (1) can be written in nondimensional form as follows :

$$\frac{h^2}{\mu_w u_{*sw}} \frac{dP}{dx} = R_{*s}\,(1 + \eta) \tag{2}$$

where $\eta = \tau_{bw}/\tau_{sw}$ is the bottom to surface shear stress ratio, $u_{*sw} = (\tau_{sw}/\rho_w)^{1/2}$ is the water shear velocity at the interface, μ_w is the dynamic viscosity of the water and

$$R_{*s} = \frac{u_{*sw}\, h}{\nu_w} \tag{3}$$

is the Reynolds number of the wind-induced flow expressed in terms of the water shear velocity at the interface, the water depth h and the kinematic viscosity of the water $\nu_w = \mu_w/\rho_w$. Since the shear stress exerted by the air on the water surface must be continuous across the interface, the water shear velocity u_{*sw}, is given by [15]

$$u_{*sw} = \left(u_{*sa}^2 - \frac{\tau_{wd}}{\rho_a} \right)^{\frac{1}{2}} \left(\frac{\rho_a}{\rho_w}\right)^{\frac{1}{2}} = \left(\frac{\tau_{sw}}{\rho_w}\right)^{\frac{1}{2}} \tag{4}$$

in which ρ_a is the air density, $u_{*sa} = (\tau_{sa}/\rho_a)^{1/2}$ is the air shear velocity at the interface, τ_{sa} is the air shear stress at the interface and τ_{wd} is the momentum flux extracted by long waves due to the growth of waves in the wind direction, the so-called wave drag [17].

The presentation of mean velocity data in the neighborhood of the shearing wall, in terms of the coordinates of the universal inner law of velocity distribution, involves the wall shear stress. The logarithmic portion of the velocity profile is given by

$$\frac{u_{sw} - \bar{u}_w}{u_{*sw}} = A \log \frac{(h - z)\, u_{*sw}}{\nu_w} + B \tag{5}$$

in which u_{sw} is the Lagrangian surface velocity or the so-called drift velocity, z is the upwards vertical coordinate from the lake bottom, see Fig. 1b, $\bar{u}_w$ is the mean water velocity at a distance (h-z) from the still water surface, $(u_{sw} - \bar{u}_w)$ is the current relative to the water surface and A and B are constants determined by the slope of the logarithmic profile and the state of the interface, respectively. The constant A is equal to $2.30/\kappa$ where κ is the von Kármán constant (a common value of κ is equal to 0.4 which results in a value of constant A equal to 5.75) and the constant B is equal to 5.5 and -2.1 for hydrodynamically smooth and fully rough condition, respectively [11].

The position of zero velocity, i.e., $\bar{u}_w = 0$ at z = h - z_v or at $z_h = 1 - z_{vh}$ in terms of the nondimensional vertical coordinate $z_h = z/h$, i.e., $(z_{vh} = z_v/h)$, for Reynolds number $R_s = u_{sw} h/\nu_w$ expressed in terms of surface velocity, greater than approximate 5×10^3, is on the logarithmic portion of the velocity profile. The value of z_{vh} is equal to 1/3 for the laminar flow case and presumes values as low as 1/6 for the turbulent flow case [13].

Thus, for $z = h - z_v$, Eq. (5) yields

$$\frac{u_{sw}}{u_{*sw}} = A \log \frac{z_v u_{*sw}}{\nu_w} + B \tag{6}$$

or in terms of the Reynolds number R_s

$$\frac{u_{sw}}{u_{*sw}} = A \log(R_s \frac{u_{*sw}}{u_{sw}} z_{vh}) + B \tag{7}$$

From the definition of the nondimensional skin friction coefficient c_f,

$$c_f = \frac{\tau_{sw}}{\rho_w u_{sw}^2/2} \tag{8}$$

it follows that

$$c_f = 2 (\frac{u_{*sw}}{u_{sw}})^2 \tag{9}$$

Combining Eq. (7) and (9) yields

$$(\frac{2}{c_f})^{1/2} = A \log (R_s (\frac{c_f}{2})^{1/2}) + B + A \log (z_{vh}) \tag{10}$$

or in terms of R_{*s}

$$(\frac{2}{c_f})^{1/2} = A \log (R_{*s}) + B + A \log (z_{vh}) \tag{11}$$

The nondimensional wind set-up in terms of the drift velocity u_{sw} is given by

$$\frac{h^2}{\mu_w u_{sw}} \frac{dP}{dx} = \frac{c_f}{2} R_s (1 + \eta) \tag{12}$$

Finally introducing the Froude number of the wind-induced fluid motion [7], [9]

$$Fr = \frac{u_{sw}}{(gh)^{1/2}} \tag{13}$$

Eq. (12) becomes

$$\frac{1}{Fr^2} \frac{1}{\rho_w g} \frac{dP}{dx} = (\frac{c_f}{2}) (1 + \eta) \tag{14}$$

The above expressions for the skin friction coefficient and the nondimensional pressure gradient will be compared later in this paper with laboratory and field experimental results.

EXPERIMENTAL APPROACHES

Air-water tunnels were used in [1],[2], [14] and [4] in order to simulate the wind-induced currents. The wind set-up was calculated by balancing the pressure and shear forces. A photographic method using spherical shaped particles was used in [1], slightly buoyant spherical particles and thin disks in [14] and laser-doppler velocimetry in [2] and [4] for the mean velocity measurements. The surface shear stress was obtained directly from the static pressure drop in the air passage of the wind-water tunnel [1], from the logarithmic velocity profile in both air and water sides [14] and [4] and from direct measurements of shear stress close to the interface [2]. Solid-air models were used in [6] and [13], a belt-type system in [6] and a moving air volume contained in a bottomless box above a

stationary bench in [13]. Hot-film anemometry was used in [6] and hot-wire anemometry in [13] for mean velocity measurements. The shear stresses were determined from the logarithmic velocity profile in [6] and from the velocity gradient in the viscous sublayer in [13]. In field studies in lakes St. Clair [10], Erie [5] and Ontario [3] the wind set-up was measured directly with water level gauges.

RESULTS AND DISCUSSION

Experimental results obtained from the laboratory and field studies are in good agreement with Eq. (2) as illustrated in Fig. (2) for three values of η, i.e., 0.0, 0.1 and 0.2 reflecting the balance of the shear and pressure forces. Another presentation of these results is in terms of surface velocity which can be related to wind velocity [14] as follows :

$$u_{sw} = \alpha U_{10} \tag{15}$$

where U_{10} is the wind speed measured 10 m above the mean water level in the field studies and 10 cm in the laboratory studies and α is a constant with a commonly accepted value of 0.03 [14] and is relative insensitive to fetch [8], with R_s, and is given in Fig. 3. The skin friction coefficient c_f for hydrodynamically smooth and fully rough conditions is determined by means of Eq. (10) with A = 5.75 and B = 5.5 and -2.1 respectively,

$$\left(\frac{2}{c_f}\right)^{1/2} = 5.75 \log \left(R_s \left(\frac{c_f}{2}\right)^{1/2}\right) + 5.5 + 5.75 \log (z_{vh}) \tag{16}$$

$$\left(\frac{2}{c_f}\right)^{1/2} = 5.75 \log \left(R_s \left(\frac{c_f}{2}\right)^{1/2}\right) - 2.1 + 5.75 \log (z_{vh}) \tag{17}$$

where the value of the constant B = -2.1 corresponds to a roughness Reynolds number $R_k = u_{*sw}\, k/\nu_w = 70$, k is the roughness length of the water-side shear layer. The curves (F_1) and (F_2) are plots of Eqs. (12) for $\eta = 0.1$ and two values of z_{vh}, i.e., 0.2 and 0.33, while the different symbols represent experimental points from the laboratory and field experiments. The experiments from [2] are adjusted for consistency using the Lagrangian surface velocity which is 3% of the wind speed rather than the Eulerian velocity which is about 2% of the wind speed. This diagram shows that most of the results from the laboratory and field studies lie between the theoretical curves (F_1) and (F_2) in Fig. 3, which represent the smooth and rough surface conditions for these Reynolds numbers. This is proof for the transitionally rough state of the air-water interface apart from occasions where it is fully rough mainly due to wave breaking in which case the entire concept of the roughness length is questionable [16].

The nondimensional pressure gradient involving the Froude number of the induced flow, according to Eq. (14) for hydrodynamically smooth and fully rough conditions is given in Fig. 4 together with the results from laboratory and field experiments. This presentation shows the transitionally rough nature of the air-water interface and the relative insensitivity of the nondimensional pressure gradient to Reynolds number and surface roughness [9].

Finally, the skin friction coefficient c_f as a function of Reynolds number R_s is presented in Fig. 5 from the laboratory and field studies (the skin friction for the field experiments is determined by equating shear and pressure forces using a cross-sectionally averaged depth by means of Eq. 12) together with analytical solutions based on logarithmic velocity profiles for the smooth and rough regime, i.e., Eqs. (16) and (17) for three values of

z_{vh}, i.e., 0.20, 0.25 and 0.33. This presentation also illustrates that the majority of the experimental results lie in the transitionally rough regime although it seems that the present analysis underestimates both wind set-up and skin friction coefficient for Reynolds numbers R_s greater than 1×10^6 when it is compared with the field results. One possibility is that the slope of the logarithmic profile is lower than 5.75 possibly due to the wave dynamics, especially in cases where the RMS of the wind-induced velocity component $\tilde{u}$ is larger than the RMS of the fluctuating velocity component u' [2]. This is shown in Fig. 5 by the curve (F_3) where the skin friction coefficient is calculated by means of the following equation

$$(\frac{2}{c_f})^{1/2} = 5.11 \log (R_s (\frac{c_f}{2})^{1/2}) - 2.1 + 5.11 \log (z_{vh}) \qquad (18)$$

which is equivalent to Eq. (17) with a milder slope of the logarithmic velocity profile (A = 5.11 corresponds to $\kappa = 0.45$) and $z_{vh} = 0.20$. The other possibility is that the air-water interface is fully rough with B < -2.1. This is also shown by the curve (F_4) which is the plot of the equation similar to Eq. (16) with B = -4.0 which corresponds to a roughness Reynolds number $R_k = 150$ and $z_{vh} = 0.20$. A combination of the above possibilities for $\kappa = 0.50$ and $R_k = 100$ yields the curve (F_5) which is the plot of Eq. (10) with A = 4.60, B = -2.6 and $z_{vh} = 0.20$. A change of constants A and B by 20% causes an up to 45% and 6% change in the value of the skin friction coefficient, respectively. This demonstrates that the present analysis is more sensitive to the changes of the slope of the logarithmic profile rather than the state of the air-water interface. Finally, it is evident from Fig. 6 that the laboratory and field values of skin friction coefficient are inside an envelope consisted by the curves (F_1) and (F_5) except the results from Lake Erie [5] and [7] which are above this range. The reasoning for this discrepancy is due to the fact that the water surface displacement is inverse proportionally to the local depth and is sensitive to large irregularities present in both depth and plan of the lake. As a result an error is introduced when a cross-sectionally averaged depth is used for the calculation of the skin friction coefficient from the wind set-up, which is more pronounced in long shallow lakes (Lake Erie) [5] rather than in short narrow (Lake St. Clair) [10] and long deep lakes (Lake Ontario) [3].

A relation between skin friction coefficient and aerodynamic drag coefficient defined as [3], $C_d = \tau_{sa}/(\rho_a U_{10}^2)$, can be provided by using Eqs. (4) and (15) and the relation between wave drag and air shear stress at the interface $\tau_{wd} = \beta \tau_{sa}$ where β has a value around 0.2 in the field [12], [17] and is as high as 0.5 in the laboratory [4], [8]. This results in

$$C_d = \frac{\rho_w \alpha^2}{2\rho_a (1-\beta)} c_f \qquad (19)$$

which becomes $C_d = 0.47\, c_f$ for the field and $C_d = (0.47 - 0.75)\, c_f$ for the laboratory. Using the above relations the aerodynamic drag coefficient can be determined and is presented in Fig. 6 as a function of Reynolds number R_s.

The above results can be used by engineers for calculation of the wind set-up and the aerodynamic drag coefficient C_d. A simple example is presented herein. Suppose the steady state wind set-up and the aerodynamic drag coefficient C_d is to be estimated for a lake 200 km long and 20 m deep (cross-sectionally averaged depth) for a wind speed of $U_{10} = 10$ m/s. The drift velocity u_{sw} can be calculated using Eq. (15) with $\alpha = 0.03$. From Figs. 3 or 4, after calculating the Reynolds number R_s and assuming negligible variations of the atmospheric pressure, one can then calculate the values of the wind set-up for the smooth and fully rough conditions. In the above case the wind set-up lies

between 9 cm and 16 cm. From Fig. 6 one can determine the values for the drag coefficient C_d for the smooth and fully rough conditions. In the above cases the values of the drag coefficients C_d are 0.90×10^{-3} and 1.55×10^{-3}, respectively. In the present case due to the high wind speed, it is more likely to have a rough air-water interface with $B < -2.1$ and probably a milder velocity profile slope. An example using the values from curves (F_4) and (F_5) yields for the wind set-up, 17.5 cm and 24.5 cm, and for the drag coefficient C_d 1.75×10^{-3} and 2.40×10^{-3}, respectively.

The present analysis does not involve a direct fetch and wind velocity dependence on the drag coefficient; it is known that in the field the drag coefficient decreases with increasing fetch and increases with increasing velocity [16] while in the laboratory the drag coefficient due to the short fetches is much larger than that determined in the field with long fetches and increases with increasing velocity [14] and fetch [8]. Also, knowing that whitecapping occurs at wind velocities higher than 8.5 m/s in the laboratory [14] and higher than 7 m/s in the field (visual observations) and that the air-water interface conditions are smoother for longer fetches one can use for the calculation of the drag coefficient and wind set-up; the values between curves (F_1) and (F_2) for velocities between 2.5 to 8.5 m/s and between curves (F_2) and (F_5) for velocities higher than 8.5 m/s in the laboratory; the values closer to the curve (F_1) with $\eta = 0.1$ for long fetches and velocities less than 7 m/s in the field and between curves (F_2) and (F_3) or (F_4) for velocities higher than 7 m/s. For more accurate determination of the value of the drag coefficient more experiments are required in order to provide information about the slope of the velocity profile for high velocities and long fetches and on the proper roughness height to be used for the wind set-up determination.

CONCLUSIONS

A new analytical approach for calculating the wind set-up and the drag coefficient is presented and successfully compared with field and laboratory results.

REFERENCES

[1] Baines, W.D., and Knapp, D.J., Wind Driven Water Currents, *Journal of the Hydraulics Division* (ASCE), Vol. 91, No. HY2, pp. 205-221, 1965.

[2] Cheung, T.K., A Study of the Turbulent Layer in the Water at an Air-water Interface, Technical Report No. 287, Stanford University, Department of Civil Engineering, 1985.

[3] Donelan, M., Elder, F.C. and Hamblin, P.F. (1974), Determination of the Aerodynamic Drag Coefficient from Wind Set-up (IFYGL), *Proc. 17th Conference Great Lakes Research*, pp. 778-788, 1974.

[4] Goossens, L.T., van Pagee, H.J.A. and Tessel, P.J., Vertical Diffusion in Air Driven Water Flows, *Journal of the Hydraulics Division* (ASCE), Vol. 108, No. HY2, pp. 995-1009, 1982.

[5] Hamblin, P.F. Meteorological Forcing and Water Level Fluctuations on Lake Erie, Chapter 2.2, Lake Erie Volume, National Water Research Institute, Burlington, Ontario, Canada, 1986 (unpublished).

[6] Huey, L.J. and Williamson, J.W., Plane Turbulent Couette Flow with Zero Netflow, *Journal of Applied Mechanics*, (ASME), pp. 885-890, 1974.

[7] Keulegan, G.H., Wind Tides in Small Closed Channels, *Journal of Research, National Bureau of Standards*, Vol. 46, pp. 358-381, 1951.

[8] Lin, J.T and Gad-El-Hak, M., "Turbulent Current Measurements in a Wind-Wave Tank", *Journal of Geophysical Research*, Vol. 89, No. C1, pp. 627-636, 1984.

[9] Leutheusser, H.J. and Tsanis, I.K., "Dependance of Wind Set-up on Reynolds Number of Induced Flow" accepted for presentation in the 22th Congress of *International Association for Hydraulic Research, Lausanne*, Switzerland, August 31-September 4 1987.

[10] Simons, T.J. and Schertzer, W.M., Modelling Wind-induced Water Set-up in Lake St. Clair, Contribution #87-10, Lakes Research Branch, National Water Research Institute, Burlington, Ontario, Canada, 1987 (unpublished).

[11] Schlichting, H., *Boundary Layer Theory*, 6th edition, pp. 581-583, McGraw-Hill, New York, 1968.

[12] Stewart, R.W., The Wave Drag of Wind Over Water, *Journal of Fluid Mechanics*, Vol. 10, pp. 189-190, 1961.

[13] Tsanis, I.K., Characteristics of Shear-induced Countercurrent Flow, Doctoral Thesis, Department of Civil Engineering, University of Toronto, Canada, 1986.

[14] Wu, J., Wind-Induced Drift Currents, *Journal of Fluid Mechanics*, Vol. 68, part 1, pp. 49-70, 1975.

[15] Wu, J., Prediction of Near-surface Drift Currents from Wind Velocity, *Journal of the Hydraulics Division* (ASCE), Vol. 99, pp. 1291-1302, 1973.

[16] Wu, J., Wind-stress Coefficients over Sea Surface near Neutral Conditions - A Revisit, *Journal of Physical Oceanography*, Vol. 10, pp. 727-740, 1981.

[17] Wu, J., Roughness Elements of the Sea Surface - Their Spectral Composition, *Tellus 38A*, pp. 178-188, 1986.

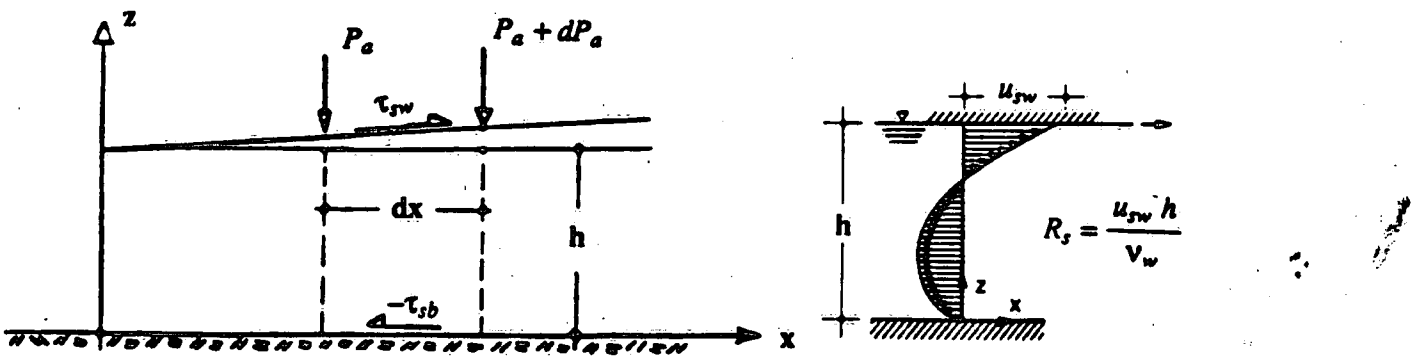

Fig. 1: Definition Diagram of Wind Set-up and Wind-induced Currents

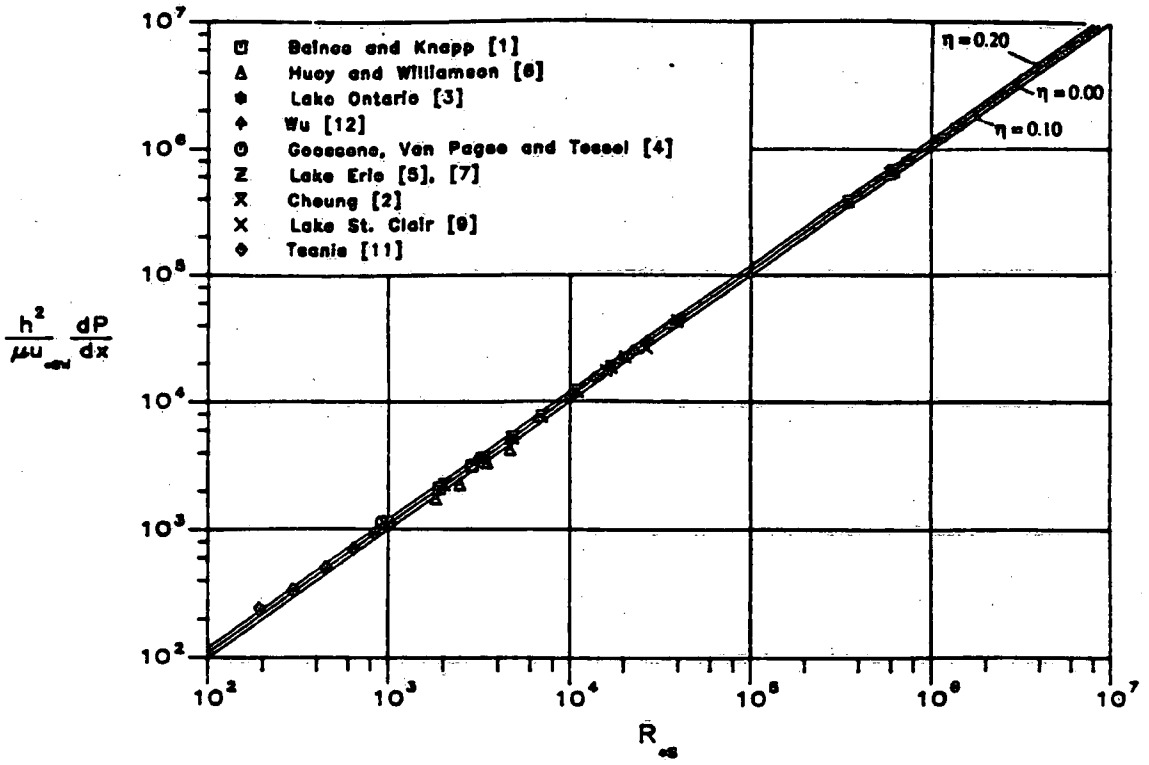

Fig. 2: Nondimensional Pressure Gradient as a Function of Reynolds Number R_{*_s}

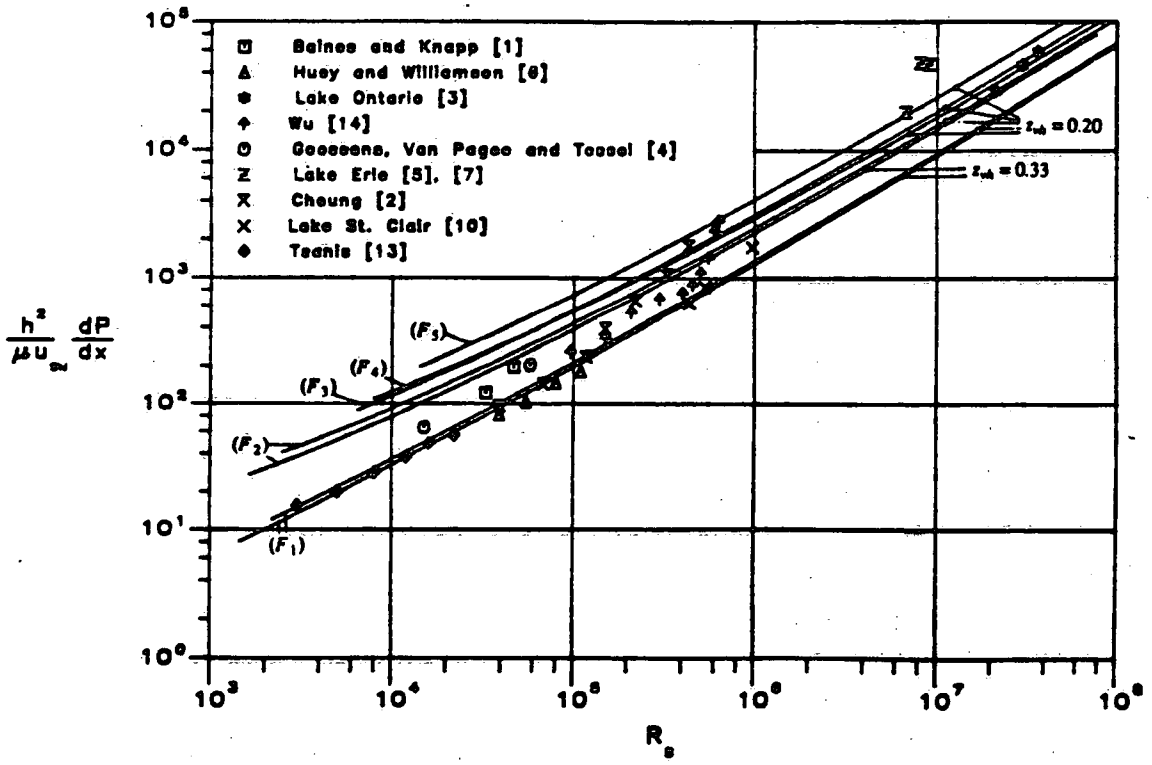

Fig. 3: Nondimensional Pressure Gradient as a Function of Reynolds Number R_s

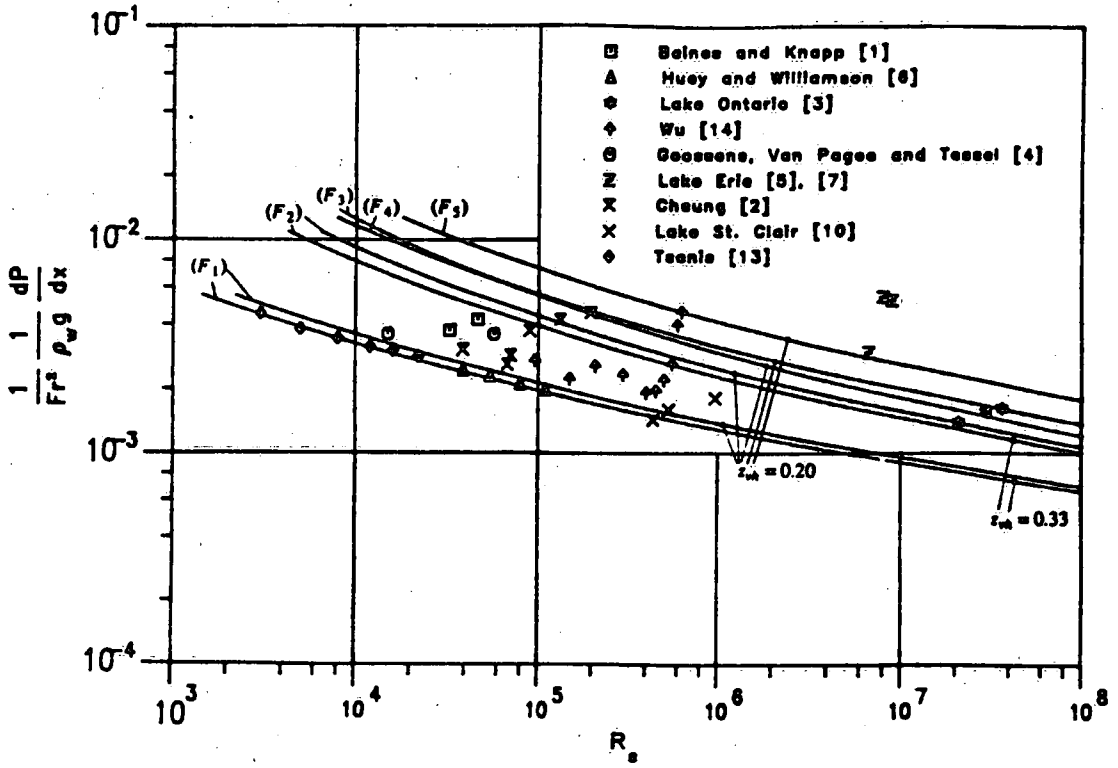

Fig. 4: Nondimensional Wind Set-up as a Function of Reynolds Number R_s

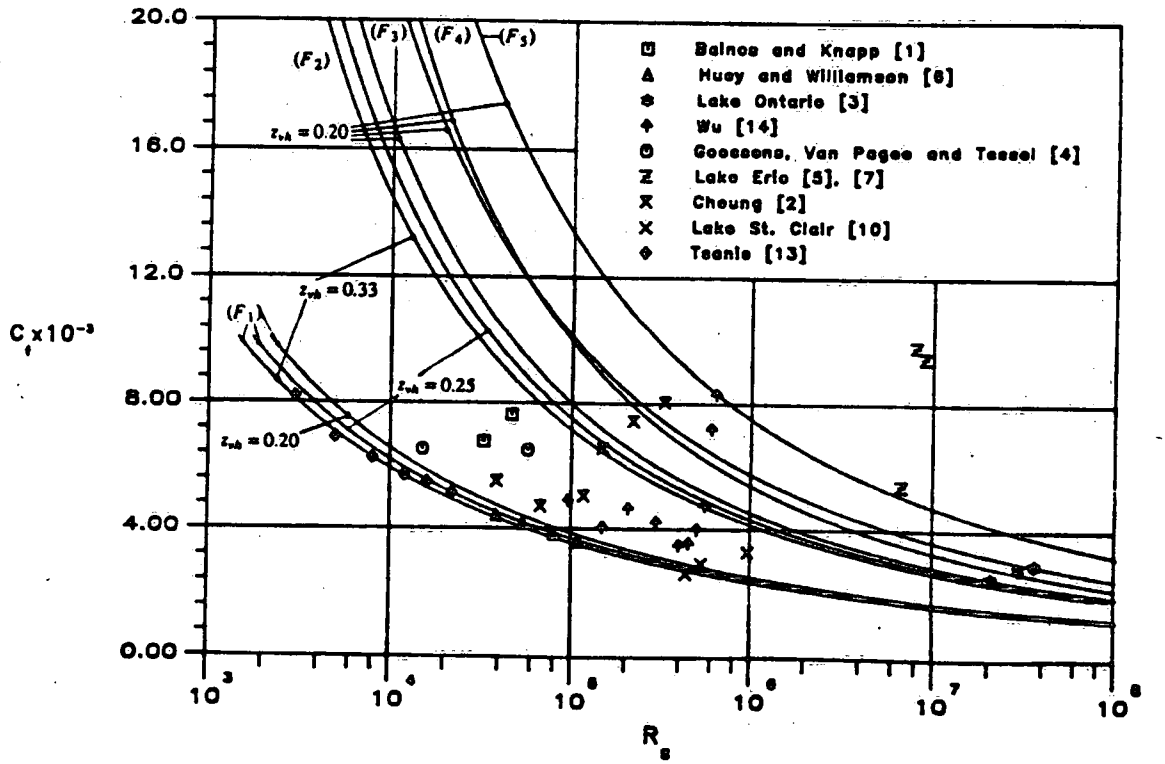

Fig. 5: Skin Friction Coefficient c_f as a Function of Reynolds Number R_s

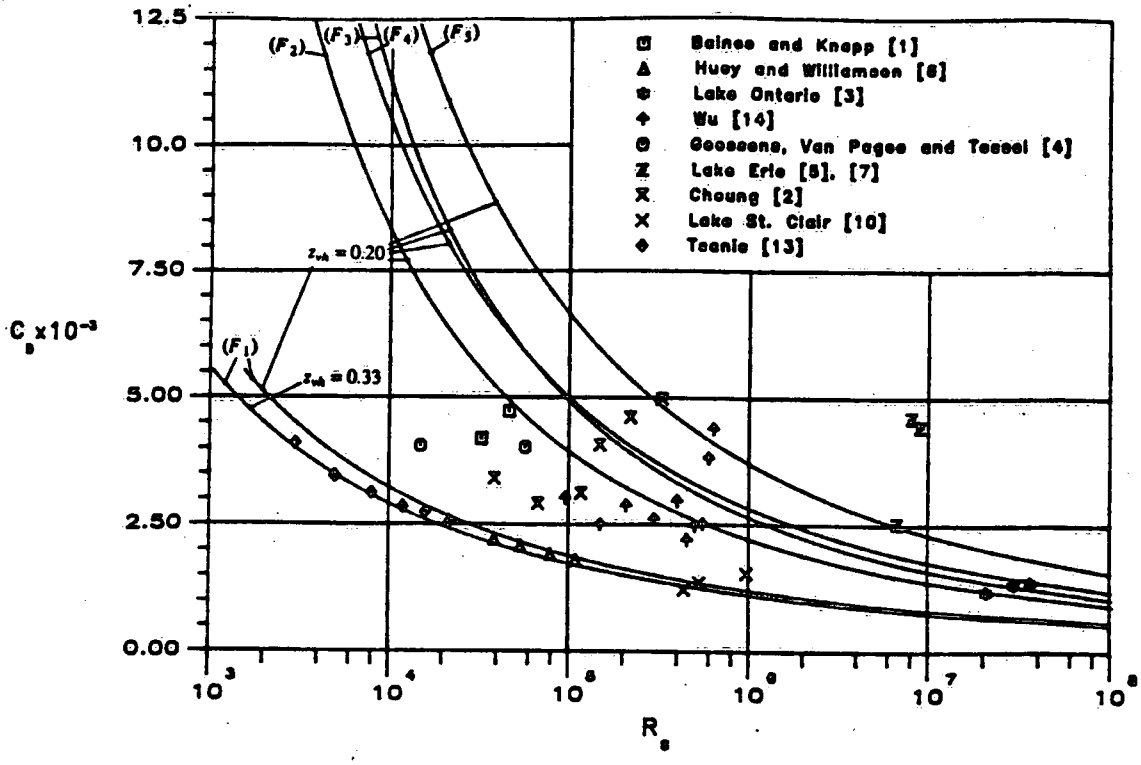

Fig. 6: Drag Coefficient C_d as a Function of Reynolds Number R_s